Progress in Neuropsychopharmacology & Biological Psychiatry 131 (2024) 110956

Contents lists available at ScienceDirect

Progress in Neuropsychopharmacology & Biological Psychiatry

journal homepage: www.elsevier.com/locate/pnp

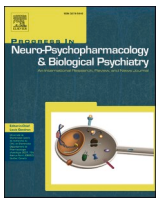

Resolving heterogeneity in dynamics of synchronization stability within the salience network in autism spectrum disorder

Xiaonan Guo [a,b,*], Xia Zhang [a,b], Junfeng Liu [c], Guangjin Zhai [a,b], Tao Zhang [a,b], Rongjuan Zhou [d], Huibin Lu [a,b], Le Gao [a,b,*]

[a] School of Information Science and Engineering, Yanshan University, Qinhuangdao 066004, China
[b] Hebei Key Laboratory of Information Transmission and Signal Processing, Yanshan University, Qinhuangdao 066004, China
[c] Department of Neurology, West China Hospital, Sichuan University, China, Chengdu, 610041, China
[d] Maternity and Child Health Hospital of Qinhuangdao, Qinhuangdao 066000, China

ARTICLE INFO

Keywords:
Autism spectrum disorder
Salience network
Synchronization stability
Heterogeneity
Resting-state functional magnetic resonance imaging

ABSTRACT

Background: Heterogeneity in resting-state functional connectivity (FC) are one of the characteristics of autism spectrum disorder (ASD). Traditional resting-state FC primarily focuses on linear correlations, ignoring the nonlinear properties involved in synchronization between networks or brain regions.
Methods: In the present study, the cross-recurrence quantification analysis, a nonlinear method based on dynamical systems, was utilized to quantify the synchronization stability between brain regions within the salience network (SN) of ASD. Using the resting-state functional magnetic resonance imaging data of 207 children (ASD/typically-developing controls (TC): 105/102) in Autism Brain Imaging Data Exchange database, we analyzed the laminarity and trapping time differences of the synchronization stability between the ASD subtype derived by a K-means clustering analysis and the TC group, and examined the relationship between synchronization stability and the severity of clinical symptoms of the ASD subtypes.
Results: Based on the synchronization stability within the SN of ASD, we identified two subtypes that showed opposite changes in synchronization stability relative to the TC group. In addition, the synchronization stability of ASD subtypes 1 and 2 can predict the social interaction and communication impairments, respectively.
Conclusions: These findings reveal that ASD subgroups with different patterns of synchronization stability within the SN appear distinct clinical symptoms, and highlight the importance of exploring the potential neural mechanism of ASD from a nonlinear perspective.

1. Introduction

Autism spectrum disorder (ASD) is an early-onset neurodevelopmental condition that exhibits dysfunctions in social interaction and communication, as well as repetitive stereotypical behaviors (American Psychiatric Association, 2013). The prevalence of ASD has been on the rise, from about 1 in 59 children with the condition in 2014 to about 1 in 36 children in 2020 (Baio et al., 2018; Maenner et al., 2023). This makes it imperative that we accelerate investigations into the underlying neural mechanisms of ASD. Converging evidence has also suggested that prominent social cognitive deficits in ASD are associated with damaged network-level intrinsic functional connectivity (FC), including the salience network (SN) (Abbott et al., 2016; Uddin et al., 2013).

The SN, which contains regions in bilateral anterior insula (AINS) and dorsal anterior cingulate cortex (ACC), is considered to participate in the process of integrating external sensory stimuli and internal states, as well as the cognitive control to guide flexible behavior (Seeley et al., 2007). Additionally, the SN has been demonstrated to play a role in switching between internally (e.g., default mode) and externally focused networks (e.g., central executive) and in regulating both task-positive and task-negative networks (Chang and Glover, 2010; Menon and Uddin, 2010). Individuals with ASD were reported to have abnormal activation patterns in regions of SN, for example, children with ASD exhibited greater activation in the right AINS than typically-developing controls (TC) during social and non-social attention (Odriozola et al., 2016). Notably, Uddin et al. uncovered that the SN have the highest accuracy in classifying individuals with ASD from TC by comparison

* Corresponding authors.
E-mail addresses: guoxiaonan@ysu.edu.cn (X. Guo), gaole@ysu.edu.cn (L. Gao).

https://doi.org/10.1016/j.pnpbp.2024.110956
Received 6 May 2023; Received in revised form 16 January 2024; Accepted 28 January 2024
Available online 1 February 2024

with other resting-state networks (Uddin et al., 2013). Furthermore, impaired FC of SN during the development of ASD has been increasingly reported (Green et al., 2016; Margolis et al., 2019; Uddin et al., 2013). A large number of studies on FC have demonstrated that FC of the SN is generally increased in children with ASD relative to TC (Margolis et al., 2019; Uddin et al., 2013). However, decreased FC has also been identified within this network of ASD aged 12–20 years (Ebisch et al., 2011; Uddin, 2015). These inconsistent findings are likely to be brought about by developmental factors or regional specificity (Menon et al., 2020; Nomi and Uddin, 2015), which highlights the high heterogeneity of ASD. The heterogeneity of ASD is also reflected in the genetics as well as the clinical phenotype (Syriopoulou-Delli and Papaefstathiou, 2019; Toma, 2020), thus increasing the difficulties in clinical diagnosis and treatment of ASD.

Resting-state FC depends on the spontaneous low-frequency fluctuations in the blood oxygenation level-dependent (BOLD) signal, reflecting synchronization in spontaneous activities between brain regions that are spatially distributed but functionally connected (Azeez and Biswal, 2017). Neuroimaging studies of ASD brains have reported disrupted neural synchronization between brain regions (Barttfeld et al., 2011; Uhlhaas and Singer, 2012). Furthermore, an fMRI study applying granger causality analysis showed atypically stable temporal alterations of FC in individuals with ASD (Uddin et al., 2015). The suggestion that the integration process is mediated by frequent transitions between different brain states has been demonstrated in neuroimaging studies (Shine et al., 2016). Therefore, the stability of the synchronization between brain regions in ASD may affect the functional integration process, resulting in atypical clinical symptoms in ASD. However, conventional analysis methods of resting-state FC is based on the linear correlation technique, ignoring the information of temporally lagged and nonlinear characteristics in the process of signal synchronization between brain regions (Bianciardi et al., 2007; Hlinka et al., 2011; Rangaprakash et al., 2013). Moreover, accumulating evidence has recognized the brain as a complicated nonlinear dynamic system (Vyas et al., 2020). Therefore, a nonlinear analysis method, known as cross-recurrence quantification analysis (CRQA), was adopted to better uncover the potential neural mechanism of ASD.

In recent years, CRQA has been extensively used in the analysis of physiological signals, such as electroencephalogram signal (Heunis et al., 2018), cardiac dynamics (Almeida et al., 2019) and behavioral features associated with ASD (Grossekathofer et al., 2017). CQRA describes the evolution of one region depending on another brain region (i.e., synchronization) over time and provides a detailed temporal and spatial description of the dynamic nature of the interaction between brain regions (Curtin et al., 2022; Kaboodvand et al., 2020; Marwan et al., 2007). Notably, CRQA also overcomes the strict requirements on the length and stable state of time series, and can intuitively disclose the dynamic evolution law of synchronization between brain regions. CRQA can directly quantify the inherent stability of synchronization between brain regions (i.e., LAM and TT), which can be obtained to characterize the nonlinear features of the signals. Moreover, CRQA was applied to analyze the generalized dynamic coupling of resting-state functional magnetic resonance imaging (fMRI) time series in phase-space during working memory tasks in patients with schizophrenia (Lombardi et al., 2019). To date, the nonlinear characteristics between signals in the brain regions within the SN of individuals with ASD are still unknown.

In the present study, we aimed to investigate synchronization stability between regions comprising the SN in ASD with CRQA by using 207 subjects from Autism Brain Imaging Data Exchange (ABIDE, http://fcon_1000.projects.nitrc.org/indi/abide/) database, including 105 ASD and 102 demographically-matched TC. Specifically, we first calculated indices (i.e., laminarity [LAM] and trapping time [TT]) characterizing the synchronization stability of interregional signal of ASD and TC groups by CRQA, and performed a K-means clustering analysis on individuals with ASD in the light of these indices to obtain ASD subtypes. Subsequently, the differences of LAM and TT among ASD subtypes and TC were analyzed. Besides, the relationships between synchronization stability (i.e., LAM and TT) and clinical symptoms of ASD subtypes were examined. Heterogeneity of FC patterns in ASD has been demonstrated (Chen et al., 2019b; Guo et al., 2022b). Moreover, resting-state functional connectivity studies have emphasized that atypical functional circuits of the right AINS are associated with symptoms in the social domain of ASD (Abbott et al., 2016; Guo et al., 2019). Considering the existing related work, we predict that there are different alterations in synchronization stability patterns within the SN in ASD that may contribute to the different clinical symptoms in the social domain of ASD.

2. Materials and methods

2.1. Participants

The resting-state fMRI data derived from ABIDE I and ABIDE II databases were used in this study (Di Martino et al., 2017; Di Martino et al., 2014). The criteria for the selection of participants were the same as in our previous work (Guo et al., 2020; Guo et al., 2022a; Guo et al., 2022b). First, we selected male children between the ages of 7 and 12 (Reams of studies have reported the existence of gender differences in individuals with ASD, such as in behavioral characteristics, brain structure and FC level (Alaerts et al., 2016; Deng and Wang, 2021; Napolitano et al., 2022; Schaer et al., 2015). Because over 90% of the participants in the dataset are male, and small sample studies may weaken the statistical power and enhance the fails of discovering true effects (Button et al., 2013; Lombardo et al., 2019), we excluded a small number of female subjects in this study to eliminate the potential impact brought by gender). Second, individuals who have valid information about full-scale intelligence quotient (FIQ), handedness, and eye status (eyes open/closed) were included. Subsequently, subjects with excessive head motion (i.e., motion exceeding 2 mm translation and 2 degrees of rotation and >50% frames with large frame-wise displacement [FD]) and without complete cortical coverage were excluded in the resting-state scan. Meanwhile, we also excluded individuals with incomplete brain anatomical images and the presence of visible motion artifacts. Most importantly, we obtained a well-matched dataset for ASD and TC groups within each site through data-driven algorithm, which maximizes p values of group differences in age, handedness, FIQ, eye status, and mean FD. Likewise, sites where >10 subjects were left in each group were selected after the above-mentioned screening procedure. A well-matched dataset including 207 children (ASD/TC: 105/102) from six sites was ultimately selected. Demographic information and clinical characteristic scores were summarized in Table 1. Meanwhile, information on scanner acquisition time and number of subjects excluded under each screening criterion were available in the Supplementary

Table 1
Demographics and clinical characteristics of the participants.

	ASD (n = 105)	TC (n = 102)	p value
Age (years)	10.15 ± 1.26	10.02 ± 1.38	0.48[a]
Handedness(right/left/mixed)	83/9/13	82/5/15	0.54[b]
FIQ	110.53 ± 17.42	113.78 ± 11.98	0.12[a]
Mean FD (mm)	0.17 ± 0.08	0.16 ± 0.08	0.16[a]
Eye status (open/closed)	91/14	88/14	0.93[b]
ADOS_Communication	3.13 ± 1.59	–	–
ADOS_Social	8.01 ± 2.51	–	–
ADOS_RRB	2.23 ± 1.63	–	–
ADOS_Total	11.33 ± 3.83	–	–

Abbreviations: ASD, autism spectrum disorder; TC, typically-developing controls; FIQ, the full-scale intelligence quotient; FD, frame-wise displacement; ADOS, the Autism Diagnostic Observation Schedule (available for 82 ASD subjects); RRB, restricted and repetitive behaviors; [a]: Indicates p values for two-sample t-tests; [b]: Indicates p values for χ^2 tests.

Materials (Table S1 and S2).

All children with ASD were identified with a clinical diagnosis of Autism, Asperger syndrome or unsorted Pervasive Developmental Disorder (PDD). There was the no history of mental or neurological illness in normally developing children. The local Institutional Review Boards has permitted all experimental proposals. All children enrolled in the trial offered consent forms and written informed consent signed by their parents/guardians was provided. Details of scanning information, diagnostic protocols, and ethics statements are available from: http://fcon_1000.projects.nitrc.org/indi/abide/.

2.2. Resting-state fMRI data preprocessing

Resting-state fMRI data preprocessing was carried out by the advanced edition of Data Processing Assistant for Resting-State fMRI (DPARSF A v4.1, http://rfmri.org/DPARSF) toolbox in MATLAB (Yan and Zang, 2010). The preprocessing of fMRI data was identical to our previous work (Guo et al., 2020; Guo et al., 2022a; Guo et al., 2022b), which includes: (1) discarding the first 10 time points; (2) slice-timing corrected; (3) spatial realigned (excluding subjects whose translational or rotational motion are >2 mm or 2°); (4) normalization to standard Montreal Neurological Institute (MNI) stereotaxic space and resampling to $3 \times 3 \times 3\ mm^3$; (5) smoothing with isotropic Gaussian kernel of 6 mm; (6) removing the linear trends; (7) despiking via the 3dDespike algorithm in Analysis of Functional NeuroImaging (https://afni.nimh.nih.gov/afni/); (8) regression of Friston 24 head motion parameters (Friston et al., 1996; Satterthwaite et al., 2012; Yan et al., 2013) as well as white matter and cerebrospinal fluid signals; (9) bandpass filtering (0.01–0.1 Hz). In order to reduce the unnecessary impact of head motion artifacts on following analysis, the percentage of high motion frames for each subject was also examined (Power et al., 2012). The time point of FD >0.5 mm and the previous one and following two time points of that point are marked as high-motion frames (Chen et al., 2019a). Participants with high-motion frames of <50% were incorporated in the subsequent analysis (Chen et al., 2017; Guo et al., 2019).

In this study, the regions of interests (ROIs) of the SN were 6 mm spheres centered on the MNI coordinates of the network provided by the CONN (obtained from independent component analysis of 497 subjects from the Human Connectome Project, https://www.nitrc.org/projects/conn/). The SN consists of 7 ROIs, namely, ACC, bilateral AINS, bilateral rostral prefrontal cortex (RPFC) and bilateral supramarginal gyrus (SMG), whose MNI coordinates are shown in Table 2.

2.3. Calculation of instantaneous phase

Since previous studies have illustrated increased variability in BOLD signal of ANIS within the SN (Nomi et al., 2017), and abnormal variability of BOLD signal in individuals with ASD (Easson and McIntos, 2019), in this study we converted the preprocessed BOLD signals into phase time series without accounting for their amplitude, which is less susceptible to inter-subject amplitude variation, head motions and additional noise. Originating from the calculation method of phase in reference (Glerean et al., 2012; Kaboodvand et al., 2019), the detailed calculation is as follows: (1) the Hilbert transform was applied to the BOLD signal to obtain an analytic representative of the real valued BOLD signal, as shown in eq. (1). (2) The instantaneous phase of the analytic signal is derived by calculating the four-quadrant inverse tangent ($\tan^{-1}$) of the quotient resulting from dividing the imaginary part of the BOLD signal by its real part (see Fig. 1A).

$$x_a(t) = x(t) + jH[x(t)] \tag{1}$$

Where $x(t)$ is the BOLD signal. $H[\cdot]$ is the Hilbert transform and j is the imaginary unit.

Table 2
Coordinates of regions of interest (ROIs) in the salience network (SN).

ROIs	MNI coordinates
Anterior Cingulate Cortex, ACC	0, 22, 35
Anterior Insula, AINS, left	−44, 13, 1
Anterior Insula, AINS, right	47, 14, 0
Rostral Prefrontal Cortex, RPFC, left	−32, 45, 27
Rostral Prefrontal Cortex, RPFC, right	32, 46, 27
Supramarginal Gyrus, SMG, left	−60, −39, 31
Supramarginal Gyrus, SMG, right	62, −35, 32

Notes: For SN mean time series were extracted from 6 mm spheres centered on the Montreal Neurological Institute (MNI) coordinates. The coordinates correspond to the seeds which are provided by the CONN obtained from independent component analysis of 497 subjects from the Human Connectome Project.

2.4. Construction of phase-space

For obtaining the time evolution trajectory of the signals within the SN in the phase-space, we used the method of dynamic systems, whose theory is a mathematical framework for depicting the evolution of complicated systems over time and depends on the conception of a phase-space. Remarkably, time-delay technique (based on the time-delayed values of the variables of observed system) is frequently utilized to complete phase-space reconstruction in current research (Curtin et al., 2022). The lag-delayed surrogate time series derived from each phase time series by applying Takens Embedding Theorem were exploited to construct phase-space portraits, as displayed in Fig. 1B. The process deals with the determination of two parameters (i.e., τ and m, respectively, represent the delay interval and dimension used in the reconstruction). Given the procedure described by Roulston (Roulston, 1999), we chose the lag parameter (i.e., τ) by the mutual information algorithm. Concretely, the mutual information function about τ was yielded, and the value of τ corresponding to the first minimum value of mutual information was chosen. Similarly, the false nearest-neighbors algorithm mentioned by Kennel et al. was applied to determine the embedding dimension (i.e., m), so as to construct the phase portrait with increased dimension and select the minimum m value that minimizes the false nearest-neighbors number (Kennel et al., 1992).

2.5. Cross-recurrence plot (CRP)

To explore the dependencies between two disparate systems by comparison of two system states, a bivariate extension of recurrence plot, known as the cross-recurrence plot (CRP) was proposed (Marwan and Kurths, 2002). The cross-recurrence matrix is defined as:

$$\boldsymbol{CR}_{i,j}^{\vec{x},\vec{y}}(\varepsilon) = \Theta\left(\varepsilon - \left\|\vec{x}_i - \vec{y}_j\right\|\right), i = 1,\ldots,N, j = 1,\ldots,M \tag{2}$$

where $\vec{x}_i$ and $\vec{y}_j$ represent the state-space trajectories of the two ROIs, respectively. N is the number of measured points $\vec{x}_i$, M is the number of measured points $\vec{y}_j$. ε is a threshold distance. $\Theta(\cdot)$ is the Heaviside function and $\left\|\vec{x}_i - \vec{y}_j\right\|$ denotes the distance of two state-space trajectories ($\vec{x}_i, \vec{y}_j$), which was calculated using Euclidean distance (Marwan et al., 2007).

Here, we analyzed the synchronization between ROIs via the application of CRP, yielding the measure of cross-signal synchronization in SN. After the phase of ROIs participated in the reconstruction of phase-space, the state-space trajectories generated were used for the construction of CRP (see Fig. 1C), which was carried out by the Dynamical Systems library (https://juliadynamics.github.io/DynamicalSystems.jl/latest/) in Julia (Datseris, 2018). CRP captures the time when one ROI visits a space previously occupied by another ROI, that is, a recurrence expressed at 30 time points on the x-axis and 50 time points on the y-axis points out that one ROI at time point 50 has visited the coordinates where another ROI was located at time point 30. Notably, the

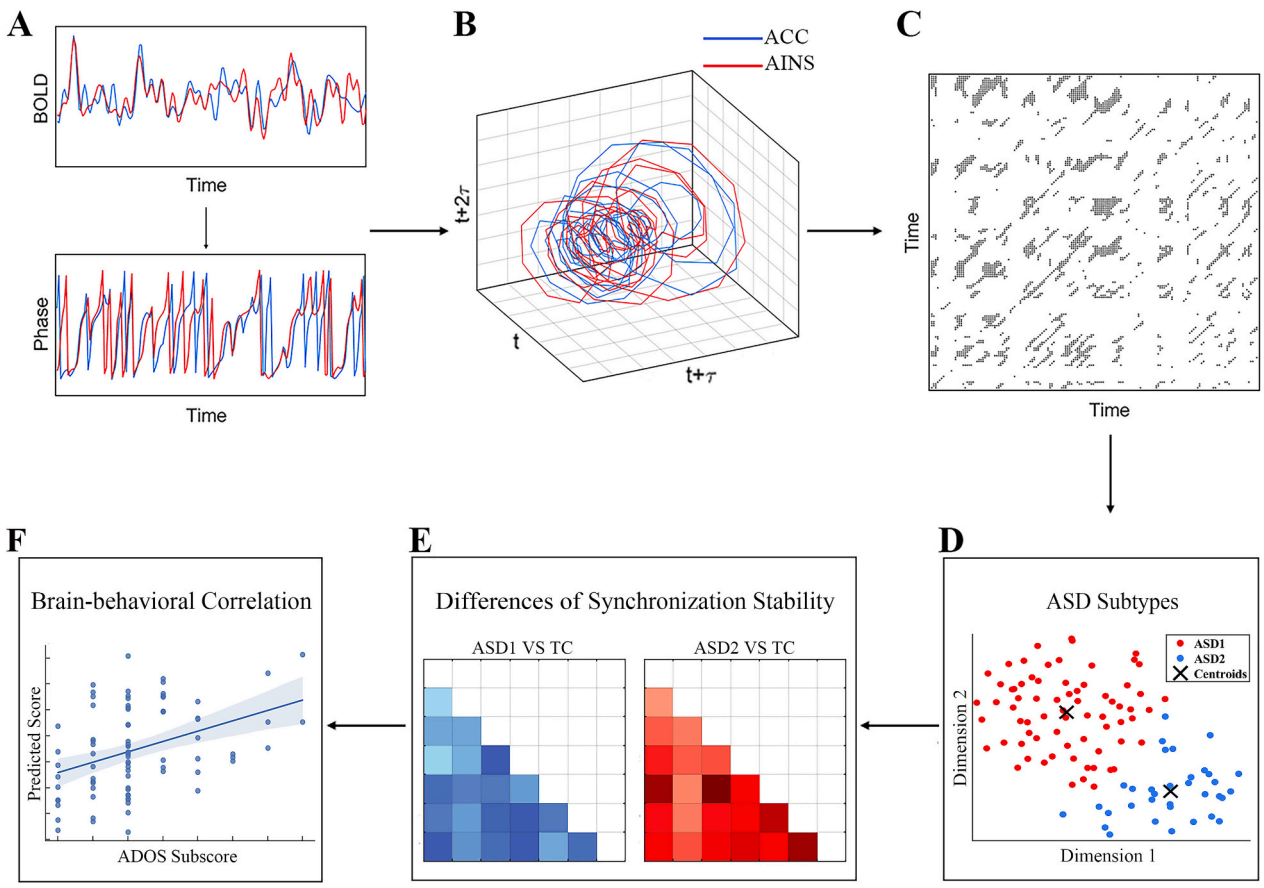

Fig. 1. The workflow for cross-recurrence quantification analysis. (A) An example of instantaneous phase time series of anterior cingulate cortex (ACC) and anterior insula (AINS) derived from Hilbert transform of its blood oxygen level-dependence (BOLD) signal. **(B)** The phase-space trajectory diagram of the phase signals shown in panel (A) is obtained according to the delay embedding of Takens. **(C)** Cross-recurrence plot originated from panel (B). **(D)** A two-dimensional schematic representation of results for autism spectrum disorder (ASD) subtypes (obtained from K-means clustering analysis based on the synchronization stability features quantified from vertical or horizontal structures in cross-recurrence plots) was completed using the t-distributed stochastic neighbor embedding algorithm. **(E)** Group differences between the resulting ASD subtypes, as well as between them and typically-developing controls (TC) group in terms of laminarity and trapping time, were analyzed by two-sample *t*-tests. **(F)** The relationship between the synchronization stability of ASD subtypes and Autism Diagnostic Observation Schedule (ADOS) subscore was also explored.

delay times of the two signals can be different, but the embedding dimensions must be the same (when unequal, the higher embedding dimension is selected).

In addition, the construction of the CRP involved the parameter ε, which determines the percentage of recurrence points in the CRP, that is, the recurrence rate (recurrence density). The recurrence rate is defined as the ratio of the number of recurrence points to the number of all points in the CRP. If the threshold ε is set too small, it may result in almost no recurrence points in the CRP, while false positives will be brought in by an overlarge threshold (Kaboodvand et al., 2020; Marwan et al., 2007). In this study, we applied the widely used relative strategy (fixed recurrence density) to determine the threshold value of this parameter. Similar to the threshold setting for this parameter in the study by Curtin et al. (Curtin et al., 2022), a recurrence rate of the CRP was fixed at 0.1 (i.e., 10%). Besides, we used more conservative (5%) and more liberal (20%) thresholding strategy to verify the stability of the results.

2.6. Recurrence quantification in state-space

The vertical (or horizontal) line structure in a CRP provides an in-depth understanding of stability in a given state-space trajectory, and represents states captured for a period of time, that is, the state does not change with time or change extremely slowly, which are regarded as an embodiment of the laminar states (Kaboodvand et al., 2020; Marwan et al., 2007). Therefore, in accordance with the presence of vertical (or horizontal) line structure, laminar states denote that the trajectories of phase between ROIs are in a stable synchronization. In this study concentrating on stability, we calculated two indexes which quantify aspects of stability in cross-signals synchronization. One is the LAM, which is determined by the ratio of recurrence points forming the vertical lines with a minimum length of ϑ_{min} (usually set to 2, that is, a pattern of repetition persisting over 2 consecutive measurements) to all observed recurrence points, describes the emergence of laminar states (i.e., the possibility that a state will not change at the next moment) during cross-signal synchronization. Another index, TT, characterizes the mean time the system is trapped in a particular state by calculating the average length of the vertical (or horizontal) structure (where ϑ_{min} was similarly set to 2), which means the duration of the stable state of cross-signal synchronization in this study. In other words, LAM and TT measure the synchronization stability of the inter-regions signals within the SN. Specifically, the larger the values of LAM and TT, the greater the stability of the signals between brain regions within the SN during the synchronization process.

2.7. Subtypes of ASD by synchronization stability

After completing the calculation of the synchronization stability indicators (i.e., LAM and TT, with 42 features in total), we first regressed the age, FIQ, mean FD, handedness, eye status and sites (using a dummy

coding scheme) from these indicators. LAM and TT were then used as the features to implement K-means clustering analysis, with the Euclidean distance, in which the average silhouette coefficient is considered as an effective indicator to evaluate clustering effect (Rousseeuw, 1987). The final clustering index (i.e., average silhouette coefficient) under each number of clusters (i.e., the range was from 2 to 20 in the analysis) is obtained by setting the number of repetitions to 100. We determined the final number of clusters by average silhouette coefficient, that is, the clustering number corresponding to the maximum average silhouette coefficient. The two-sample *t*-tests was performed on the identified ASD subtypes based on LAM and TT with age, FIQ, mean FD, handedness, eye status and sites (using a dummy coding scheme) as covariables to validate the results of our clustering analysis. The identical analysis was utilized to determine whether there were differences in those indicators between each ASD subtype and TC group. Multiple comparisons were performed using false discovery rate (FDR) correction with statistical significance of $p < 0.05$. Furthermore, the differences between ASD subtypes on data sites, ASD types, and comorbidity with other psychiatric disorders were examined by χ^2 tests, and the distribution of these variables for each subtype was analyzed. Moreover, the comparison of ADOS subscores for ASD subtype 1 and 2 was carried out by two-sample t-tests. The differences in measures of synchronization stability between the entire ASD group and the TC group were also analyzed via application of the method above.

2.8. Relationships between synchronization stability and clinical symptoms of ASD subtypes

The relationships between measures of synchronization stability (i.e., LAM and TT) in ASD subtypes and symptom severity as evaluated by Autism Diagnostic Observation Schedule (ADOS) subscores, which includes social, communication and restricted and repetitive behaviors, was then probed (Lord et al., 2000). After excluding subjects without ADOS subscores, 54 and 28 subjects from the two ASD subtypes were finally reserved for the following analysis of symptomatic prediction, respectively. A support vector regression model of the library for support vector machines (LIBSVM) package (http://www.csie.ntu.edu.tw/~cjlin/libsvm/) was applied in this analysis. In brief, we utilized support vector regression approach to model the relationship between multiple independent variables (LAM and TT of cross-signal synchronization among the ROIs in the SN, regressed covariates such as age, FIQ, mean FD, handedness, eye status and sites (using a dummy coding scheme)) and the dependent variable (ADOS subscores). Leave-one-out cross validation (LOOCV) is utilized to evaluate the performance of the model in predicting symptom severity (Schölkopf and Smola, 2018). Specifically, suppose there were n samples, after obtaining a model based on $n-1$ samples trained in each LOOCV experiment, predictions of ADOS subscores are made with the remaining one sample to evaluate the performance of the constructed model. We then calculated the correlation coefficient R between the predicted ADOS subscores yielded in light of the model after repeating the above operation n times and true ADOS subscores. The parameter setting with positive correlation coefficient was selected for nonparametric permutation test, so as to obtain the p value showing the statistical significance of the result (Golland and Fischl, 2003; Liu et al., 2015). In the permutation test, the order of the original ADOS subscores of individuals with ASD was shuffled, and the R_{perm} values were obtained based on the disrupted dataset using the same training model as in the previous step. After 1000 repetitions, the p value was determined by the ratio of the number of times that the R_{perm} value is greater than the R value to the total number of permutations (i.e., 1000).

3. Results

3.1. Significant group differences in synchronization stability

A K-means clustering analysis was performed using LAM and TT of cross-signal stability as the features, and 105 ASD was clustered into two subtypes, because the average silhouette coefficient reached the maximum value of 0.4659 when the number of clusters was two (see Supplementary Fig. S1). The results of the χ^2 tests revealed no significant differences in data sites ($\chi^2 = 0.902, p = 0.985$), ASD types ($\chi^2 = 3.09, p = 0.213$) and comorbidity with other psychiatric disorders ($\chi^2 = 0.95, p = 0.331$) between ASD subtypes. Moreover, the distribution of data sites and ASD types was examined for both ASD subtypes (Supplemental Fig. S2 and S3; see Supplementary Materials for details), and the distribution of subjects with/without other psychiatric disorders in each ASD subtype is also shown in Supplementary Materials (Fig. S4). There were no significant differences in ADOS scores between ASD subtypes 1 and 2.

To validate the results of our clustering analysis, we performed a two-sample *t*-tests on the identified subtypes based on LAM and TT. The results showed that the LAM and TT values between different ROIs in SN of subtype 1 were significantly reduced compared with subtype 2 ($p < 0.05$, FDR corrected; see Fig. 2A and D). The values of indices for each ASD subtypes and TC group were presented in Supplementary Materials (Table S3). Additionally, relative to TC group, LAM values between the right AINS, left RPFC, bilateral SMG and left AINS, and the left and right SMG were significantly decreased in ASD subtype 1 ($p < 0.05$, uncorrected; see Fig. 2B), while LAM of ASD subtype 2 was significantly increased except right RPFC-left SMG ($p < 0.05$, FDR corrected; see Fig. 2C). Similarly, the TT values between the right AINS, bilateral RPFC, bilateral SMG and left AINS in SN of ASD subtype 1 were significantly lower than in the TC group ($p < 0.05$, FDR corrected; see Fig. 2E). However, the TT values between different brain regions in SN of ASD subtype 2 showed the opposite change, that is, higher than that of TC group ($p < 0.05$, FDR corrected; see Fig. 2F). Detailed original p-values and corrected p-values of the LAM and TT of cross-signals within the SN between any two groups in the three groups (two ASD subtypes and TC group) was provided in Supplementary Materials (Table S4). The results of the retests using different parameter ε were displayed in the Supplementary Materials (Fig. S5 and 6). Besides, group comparisons between ASD and TC revealed no significant differences in LAM and TT ($p < 0.05$, FDR corrected; see Supplementary materials Table S5).

3.2. Relationships between stability of cross-signal synchronization and clinical symptoms of ASD subtypes

To investigate the relationship between stability of cross-signal synchronization (i.e., LAM and TT) and clinical symptoms of ASD subtypes, we utilized a support vector regression model and LOOCV. LAM and TT were observed to be associated with social impairments of subtype 1 ($r = 0.33, p = 0.008$; see Fig. 3A), correlated with communication impairments of subtype 2 ($r = 0.50$, $p = 0.003$; see Fig. 3B). The full results of relationships between indices and clinical symptoms of ASD subtypes were provided in Supplementary Materials (Table S6).

4. Discussion

In this study, we identified ASD subtypes by calculating indexes that characterize the stability of signal synchronization between ROIs in the SN through a nonlinear analysis method, namely CRQA, and analyzed the differences among ASD subtypes. Based on the resting-state fMRI data of ABIDE database, we found that: (1) Two ASD subtypes with different synchronization stability pattern alterations were identified, as indicated by significantly greater LAM and TT in ASD subtype 2 compared with TC group, whereas subtype 1 had lower TT between

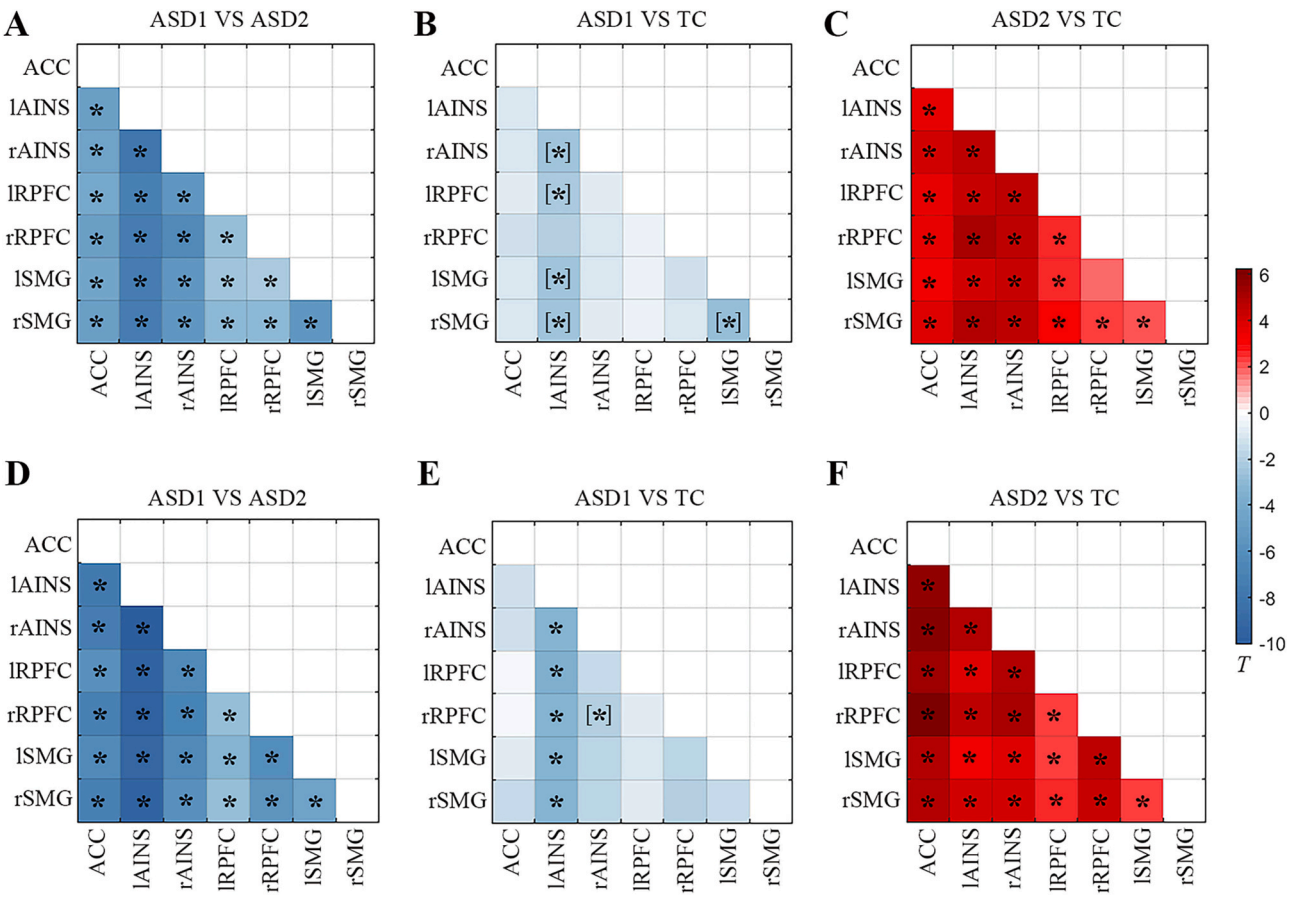

Fig. 2. Significant group differences in indices of synchronization stability. Group comparison results of laminarity between **(A)** the two ASD subgroups, **(B)** ASD subgroup 1 and TC group, as well as **(C)** ASD subgroup 2 and TC group after two-sample t-tests. Group comparison results of trapping time between **(D)** the two ASD subtypes, **(E)** ASD subtype 1 and TC group, as well as **(F)** ASD subtype 2 and TC group after two-sample t-tests. [*]indicates group differences at $p < 0.05$, uncorrected. *indicates group differences at $p < 0.05$, FDR corrected. ACC, anterior cingulate cortex; lAINS/rAINS, left/right anterior insula; lRPFC/rRPFC, left/right rostral prefrontal cortex; lSMG/rSMG, left/right supramarginal gyrus; ASD, autism spectrum disorder; TC, typically-developing controls.

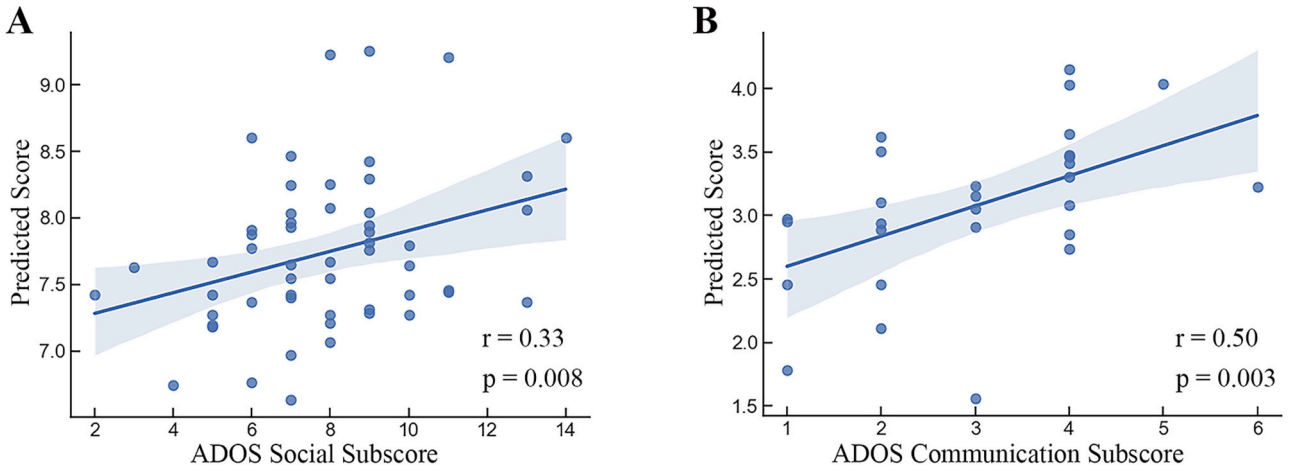

Fig. 3. Relationships between indices of synchronization stability and clinical symptoms of ASD subtypes. (A) Relationships between ADOS social subscore in ASD subtype 1 and predicted scores using indices of synchronization stability ($r = 0.33$, $p = 0.008$). **(B)** Relationships between ADOS communication subscore in ASD subtype 2 and predicted scores using indices of synchronization stability ($r = 0.50$, $p = 0.003$). ASD, autism spectrum disorder; ADOS, Autism Diagnostic Observation Schedule.

right AINS, bilateral RPFC, and bilateral SMG and left AINS than TC group. (2) LAM and TT can predict the severity of social impairments in ASD subtype 1, and the severity of communication impairments in ASD subtype 2. In summary, these results demonstrate that the altered patterns of cross-signal synchronization stability in the SN and spontaneous brain activity vary in different ASD subtypes.

These findings suggest that CRQA, a nonlinear method, contributes to explore patterns of synchronization stability within the SN in ASD and

provides new directions for studying the heterogeneity of ASD. Resting-state FC analysis mainly based on linear correlation metrics, ignoring the nonlinear features involved in the process of synchronization between brain regions. In contrast to traditional resting-state FC, this method is essentially sensitive to nonlinear and time-lagged effects, and is available on analyzing the interdependence linking one brain region to another. A recent study by Curtin et al., which applied CRQA to analysis of DMN dynamics in individuals with ASD, focused on measures of periodicity, such as determinism (Curtin et al., 2022). Nevertheless, we concentrated on analysis of stability of synchronization between brain regions in the SN, from which we obtain measures related to stability, namely frequency (i.e., LAM) and duration (i.e., TT) of stable states. CRQA quantifies the stability of synchronization between brain regions within the SN and is especially sensitive to dysregulation of synchronous activity associated with ASD. Consequently, the use of CRQA to delineate dynamics of stability in the resting-state fMRI data of ASD in this study underlines a new level of analysis. Additionally, our findings showed that synchronization stability can predict the clinical symptoms of ASD subtypes, including social interaction and communication. Abbott et al. detected that reduced FC within SN of individuals with ASD is related to sensory and socio-communicative abilities (Abbott et al., 2016). Meanwhile, a study concerning FC in the SN uncovered that increased FC between right SMG and right RPFC in ASD is associated with decreased language ability (Margolis et al., 2019). Our results are consistent with previous studies, illustrating that dysregulation of synchronization stability in the SN of individuals with ASD may lead to impairments in social and communication. Therefore, measures of stability might be a sensitive supplement to existing metrics of FC, promoting a more comprehensive cognizance of the neural mechanisms of ASD or other psychiatric diseases.

Due to the highly heterogeneous nature of individuals with ASD, in order to understand the underlying neural mechanisms of ASD and formulate accurate treatments plan, a growing number of studies analyze the heterogeneity of ASD by discriminating more homogeneous subgroups in ASD (Amaral, 2011; Kim, 2020). Despite differences in approach, a consensus suggests that there are probably at least two to four diverse ASD subtypes (Hong et al., 2020). The synchronization stability of SN of the two ASD subtypes obtained in this study was atypical and heterogeneous. Specifically, compared with TC group, the emergence and duration of stable states during synchronization within the SN were significantly increased in ASD subtype 2, suggesting increased stability and reduced variability within the SN in ASD. This finding is consistent with previous literature which found negative correlations between variability of BOLD signals and symptom severity of ASD (Easson and McIntos, 2019). Watanabe et al. explored how whole-brain neural activity patterns change over time in ASD through an energy-landscape analysis (Watanabe and Rees, 2017). The results also showed that the brains of high-functioning ASD exhibited fewer neural transitions compared to neurotypical controls, suggesting a stable pattern of brain activity in ASD (Watanabe and Rees, 2017). However, ASD subtype 1 showed decreased duration of stable states only in the synchronization between right AINS, bilateral RPFC, and bilateral SMG and left AINS. These results highlight heterogeneity in the synchronization stability patterns of SN in ASD. A study regarding the dynamic functional connectivity of the insula have shown that subregions of this structure show difference in the variability of dynamic functional connectivity (Zhao et al., 2022). Furthermore, Guo et al. found that the right AINS in ASD exhibits varied pattern of FC with other brain regions, reflecting different patterns of cooperation with other brain regions (Guo et al., 2019; Nomi et al., 2016). The variability in the connectivity states of the AINS during synchronization with other brain regions may be another source of the diverse synchronization stability patterns of ASD observed in this study.

Although the difference between ASD subtype 1 and TC group was minor, the TT between right AINS, bilateral RPFC, and bilateral SMG and left AINS of ASD subtype 1 and TC group was significantly different. Notably, in the brain behavioral analysis, we found that the stability of synchronization in SN was correlated with social impairments in ASD subtype 1. Consequently, the association of ASD subtype 1 with social deficits may result precisely from atypical duration of synchronization stability between right AINS, bilateral RPFC, bilateral SMG, and left AINS. However, there is a link between synchronization stability and communication deficits in ASD subtype 2, suggesting that different patterns of synchronization stability may lead to differences in clinical symptoms between different ASD subtypes. Thus, these findings are likely to have prominent implications for exposing the heterogeneity of ASD and are more conducive to the nosology and therapy of individuals with ASD.

In line with these results, previous studies on FC in the SN of individuals with ASD have reported incompatible findings (Ebisch et al., 2011; Margolis et al., 2019; Uddin, 2015; Uddin et al., 2013). And our findings, after excluding the influence of these factors (i.e., sex, age, FIQ), still revealed disparate patterns of synchronization stability alterations in the SN of ASD, illustrating that there may be inherent heterogeneity in patterns of synchronization stability among brain regions in the SN of ASD. Considering those results, we speculate that the inconsistencies between these reports are more likely to attributed to the existence of different ASD subtypes, so as to strengthen the investigation of ASD subtypes in the future.

4.1. Limitations

This research also has several limitations. First, the results of this study were limited to male subjects. However, gender differences in individuals with ASD have been frequently reported, and sex plays an important role in heterogeneity of ASD (Alaerts et al., 2016; Deng and Wang, 2021; Halladay et al., 2015; Lai et al., 2015; Napolitano et al., 2022; Schaer et al., 2015). Thus, future studies need to find out whether there are gender differences in synchronization stability within the SN in ASD. Second, this study only analyzed the heterogeneity of synchronization stability within the SN of children with ASD at an average age of around 10 years. However, it is not clear how synchronization stability of the SN changes in individuals with ASD at different age stages. Moreover, previous studies have manifested that age is also an important factor influencing heterogeneity in ASD (Nomi and Uddin, 2015), so longitudinal studies are necessary in the future to explore the developmental trajectory of synchronization stability in the SN of ASD. The current subtyping approach is only one of multiple approaches, such as hierarchical clustering analysis and spectral clustering analysis (Urchs et al., 2022; Wang et al., 2014); We might examine how to integrate different subtyping approaches in future studies to derive alternative perspectives on the heterogeneity of synchronization stability patterns in the SN in individuals with ASD. Lastly, considering the fact that 70% of individuals with ASD suffer from at least one comorbid psychiatric disorder, and approximately 40% suffer from two or more comorbid psychiatric disorders (Pezzimenti et al., 2019; Rim et al., 2023), whether comorbidity has an effect on ASD subtyping needs to be explored in future studies.

5. Conclusion

This study underlined the heterogeneity of synchronization stability within the SN in children with ASD. Compared with the TC group, the two ASD subtypes identified based on the heterogeneity of synchronization stability exhibited different patterns of synchronous stability changes. Moreover, the synchronization stability of the two ASD subtypes predicted different clinical symptoms of ASD. Overall, these findings manifest that the stability of synchronization between regions in the SN can be used as features of subtype analysis in ASD, emphasizing the imperative to study the nonlinear characteristics of synchronization within brain networks.

CRediT authorship contribution statement

Xiaonan Guo: Writing – original draft, Supervision, Methodology, Funding acquisition, Formal analysis, Conceptualization. **Xia Zhang:** Writing – review & editing, Writing – original draft, Visualization, Methodology, Formal analysis, Data curation. **Junfeng Liu:** Writing – review & editing, Supervision, Funding acquisition, Formal analysis. **Guangjin Zhai:** Writing – review & editing, Validation, Data curation. **Tao Zhang:** Writing – review & editing, Supervision, Funding acquisition. **Rongjuan Zhou:** Supervision, Investigation. **Huibin Lu:** Writing – review & editing, Supervision. **Le Gao:** Writing – review & editing, Supervision, Methodology, Conceptualization.

Declaration of competing interest

The authors declare that they have no known competing financial interests or personal relationships that could have appeared to influence the work reported in this paper.

Acknowledgements

This work was funded by the National Natural Science Foundation of China (No. 62303396), Hebei Natural Science Foundation (Nos. H2021203002 and H2023203007), Funding Project for the Returned Overseas Chinese Scholars of Hebei Province of China (No. C20220334), Science Research Project of Hebei Education Department (No. BJK2024067), S&T Program of Qinhuangdao (No. 202301A001) and Hebei Key Laboratory Project (No. 202250701010046). Junfeng Liu was funded by the National Natural Science Foundation of China (No. 82371323) and Sichuan Science and Technology Program (No. 2023NSFSC1558). Tao Zhang was supported by the National Natural Science Foundation of China (No. 62176229) and Hebei Natural Science Foundation (No. F2020203010). Funding sources for the datasets comprising the 1000 Functional Connectome Project are listed at http://fcon_1000.projects.nitrc.org/fcpClassic/FcpTable.html. Funding sources for the ABIDE dataset are listed at http://fcon_1000.projects.nitrc.org/indi/abide/.

Ethical statement

All study participants provided informed consent, and the study design was approved by the appropriate ethics review board.

Appendix A. Supplementary data

Supplementary data to this article can be found online at https://doi.org/10.1016/j.pnpbp.2024.110956.

References

Abbott, A.E., Nair, A., Keown, C.L., Datko, M., Jahedi, A., Fishman, I., Muller, R.A., 2016. Patterns of atypical functional connectivity and behavioral links in autism differ between default, salience, and executive networks. Cereb. Cortex 26 (10), 4034–4045.

Alaerts, K., Swinnen, S.P., Wenderoth, N., 2016. Sex differences in autism: a resting-state fMRI investigation of functional brain connectivity in males and females. Soc. Cogn. Affect. Neurosci. 11 (6), 1002–1016.

Almeida, T.P., Unger, L.A., Soriano, D.C., Li, X., Dossel, O., Yoneyama, T., Loewe, A., Ieee, 2019. Recurrence Quantification Analysis for Investigating Atrial Fibrillation Dynamics in a Heterogeneous Simulation Setup, 2019 41ST Annual International Conference Of The Ieee Engineering In Medicine And Biology Society (EMBC), pp. 2277–2280.

Amaral, D.G., 2011. The promise and the pitfalls of autism research: an introductory note for new autism researchers. Brain Res. 1380, 3–9.

American Psychiatric Association, 2013. Diagnostic and Statistical Manual of Mental Disorders (DSM-5®). American Psychiatric Publication, Arlington (VA).

Azeez, A.K., Biswal, B.B., 2017. A review of resting-state analysis methods. Neuroimaging Clin. N. Am. 27 (4), 581–592.

Baio, J., Wiggins, L., Christensen, D.L., Maenner, M.J., Daniels, J., Warren, Z., Kurzius-Spencer, M., Zahorodny, W., Rosenberg, C.R., White, T., Durkin, M.S., Imm, P., Nikolaou, L., Yeargin-Allsopp, M., Lee, L.C., Harrington, R., Lopez, M., Fitzgerald, R. T., Hewitt, A., Pettygrove, S., Constantino, J.N., Vehorn, A., Shenouda, J., Hall-Lande, J., Braun, K.V., Dowling, N.F., 2018. Prevalence of autism Spectrum disorder among children aged 8 years - autism developmental disabilities monitoring network, 11 sites, United States. MMWR-Morbidity And Mortality Weekly Report 67 (45), 1–23.

Barttfeld, P., Wicker, B., Cukier, S., Navarta, S., Lew, S., Sigman, M., 2011. A big-world network in ASD: dynamical connectivity analysis reflects a deficit in long-range connections and an excess of short-range connections. NEUROPSYCHOLOGIA 49 (2), 254–263.

Bianciardi, M., Sirabella, P., Hagberg, G.E., Giuliani, A., Zbilut, J.P., Colosimo, A., 2007. Model-free analysis of brain fMRI data by recurrence quantification. NEUROIMAGE 37 (2), 489–503.

Button, K.S., Ioannidis, J.P., Mokrysz, C., Nosek, B.A., Flint, J., Robinson, E.S., Munafò, M.R., 2013. Power failure: why small sample size undermines the reliability of neuroscience. Nat. Rev. Neurosci. 14 (5), 365–376.

Chang, C., Glover, G.H., 2010. Time-frequency dynamics of resting-state brain connectivity measured with fMRI. Neuroimage 50 (1), 81–98.

Chen, H., Nomi, J.S., Uddin, L.Q., Duan, X., Chen, H., 2017. Intrinsic functional connectivity variance and state-specific under-connectivity in autism. Hum. Brain Mapp. 38 (11), 5740–5755.

Chen, H., Uddin, L.Q., Guo, X., Wang, J., Wang, R., Wang, X., Duan, X., Chen, H., 2019a. Parsing brain structural heterogeneity in males with autism spectrum disorder reveals distinct clinical subtypes. Hum. Brain Mapp. 40 (2), 628–637.

Chen, H., Uddin, L.Q., Guo, X.N., Wang, J., Wang, R.S., Wang, X.M., Duan, X.J., Chen, H. F., 2019b. Parsing brain structural heterogeneity in males with autism spectrum disorder reveals distinct clinical subtypes. Hum. Brain Mapp. 40 (2), 628–637.

Curtin, P., Neufeld, J., Curtin, A., Arora, M., Bolte, S., 2022. Altered periodic dynamics in the default mode network in autism and attention-deficit/hyperactivity disorder. Biol. Psychiatry 91 (11), 956–966.

Datseris, G., 2018. DynamicalSystems.Jl: a Julia software library for chaos and nonlinear dynamics. J. Open Source Softw. 3, 598.

Deng, Z.Z., Wang, S.P., 2021. Sex differentiation of brain structures in autism: findings from a gray matter asymmetry study. Autism Res. 14 (6), 1115–1126.

Di Martino, A., Yan, C.G., Li, Q., Denio, E., Castellanos, F.X., Alaerts, K., Anderson, J.S., Assaf, M., Bookheimer, S.Y., Dapretto, M., Deen, B., Delmonte, S., Dinstein, I., Ertl-Wagner, B., Fair, D.A., Gallagher, L., Kennedy, D.P., Keown, C.L., Keysers, C., Lainhart, J.E., Lord, C., Luna, B., Menon, V., Minshew, N.J., Monk, C.S., Mueller, S., Müller, R.A., Nebel, M.B., Nigg, J.T., O'Hearn, K., Pelphrey, K.A., Peltier, S.J., Rudie, J.D., Sunaert, S., Thioux, M., Tyszka, J.M., Uddin, L.Q., Verhoeven, J.S., Wenderoth, N., Wiggins, J.L., Mostofsky, S.H., Milham, M.P., 2014. The autism brain imaging data exchange: towards a large-scale evaluation of the intrinsic brain architecture in autism. Mol. Psychiatry 19 (6), 659–667.

Di Martino, A., O'Connor, D., Chen, B., Alaerts, K., Anderson, J.S., Assaf, M., Balsters, J. H., Baxter, L., Beggiato, A., Bernaerts, S., Blanken, L.M., Bookheimer, S.Y., Braden, B.B., Byrge, L., Castellanos, F.X., Dapretto, M., Delorme, R., Fair, D.A., Fishman, I., Fitzgerald, J., Gallagher, L., Keehn, R.J., Kennedy, D.P., Lainhart, J.E., Luna, B., Mostofsky, S.H., Müller, R.A., Nebel, M.B., Nigg, J.T., O'Hearn, K., Solomon, M., Toro, R., Vaidya, C.J., Wenderoth, N., White, T., Craddock, R.C., Lord, C., Leventhal, B., Milham, M.P., 2017. Enhancing studies of the connectome in autism using the autism brain imaging data exchange II. Sci Data 4, 170010.

Easson, A.K., McIntos, A.R., 2019. BOLD signal variability and complexity in children and adolescents with and without autism spectrum disorder. Dev. Cogn. Neurosci. 36.

Ebisch, S.J.H., Gallese, V., Willems, R.M., Mantini, D., Groen, W.B., Romani, G.L., Buitelaar, J.K., Bekkering, H., 2011. Altered intrinsic functional connectivity of anterior and posterior insula regions in high-functioning participants with autism Spectrum disorder. Hum. Brain Mapp. 32 (7), 1013–1028.

Friston, K.J., Williams, S., Howard, R., Frackowiak, R.S., Turner, R., 1996. Movement-related effects in fMRI time-series. Magn. Reson. Med. 35 (3), 346–355.

Glerean, E., Salmi, J., Lahnakoski, J.M., Jaaskelainen, I.P., Sams, M., 2012. Functional magnetic resonance imaging phase synchronization as a measure of dynamic functional connectivity. Brain Connect. 2 (2), 91–101.

Golland, P., Fischl, B., 2003. Permutation tests for classification: towards statistical significance in image-based studies. Inf Process Med Imaging 18, 330–341.

Green, S.A., Hernandez, L., Bookheimer, S.Y., Dapretto, M., 2016. Salience network connectivity in autism is related to brain and behavioral markers of sensory Overresponsivity. J. Am. Acad. Child Adolesc. Psychiatry 55 (7), 618–626.

Grossekathofer, U., Manyakov, N.V., Mihajlovic, V., Pandina, G., Skalkin, A., Ness, S., Bangerter, A., Goodwin, M.S., 2017. Automated Detection of Stereotypical Motor Movements in Autism Spectrum Disorder Using Recurrence Quantification Analysis. Frontiers In Neuroinformatics 11.

Guo, X.N., Duan, X.J., Suckling, J., Chen, H., Liao, W., Cui, Q., Chen, H.F., 2019. Partially impaired functional connectivity states between right anterior insula and default mode network in autism spectrum disorder. Hum. Brain Mapp. 40 (4), 1264–1275.

Guo, X., Duan, X., Chen, H., He, C., Xiao, J., Han, S., Fan, Y.S., Guo, J., Chen, H., 2020. Altered inter- and intrahemispheric functional connectivity dynamics in autistic children. Hum. Brain Mapp. 41 (2), 419–428.

Guo, X.A., Cao, Y.B., Liu, J.F., Zhang, X., Zhai, G.J., Chen, H., Gao, L., 2022a. Dysregulated Dynamic Time-Varying Triple-Network Segregation in Children with Autism Spectrum Disorder. Cerebral Cortex.

Guo, X.A., Zhai, G.J., Liu, J.F., Cao, Y.B., Zhang, X., Cui, D., Gao, L., 2022b. Inter-individual heterogeneity of functional brain networks in children with autism spectrum disorder. Mol. Autism. 13 (1).

Halladay, A.K., Bishop, S., Constantino, J.N., Daniels, A.M., Koenig, K., Palmer, K., Messinger, D., Pelphrey, K., Sanders, S.J., Singer, A.T., Taylor, J.L., Szatmari, P.,

2015. Sex and gender differences in autism spectrum disorder: summarizing evidence gaps and identifying emerging areas of priority. Mol. Autism. 6.
Heunis, T., Aldrich, C., Peters, J.M., Jeste, S.S., Sahin, M., Scheffer, C., de Vries, P.J., 2018. Recurrence quantification analysis of resting state EEG signals in autism spectrum disorder - a systematic methodological exploration of technical and demographic confounders in the search for biomarkers. BMC Med. 16.
Hlinka, J., Paluš, M., Vejmelka, M., Mantini, D., Corbetta, M., 2011. Functional connectivity in resting-state fMRI: is linear correlation sufficient? NeuroImage 54 (3), 2218–2225.
Hong, S.-J., Vogelstein, J.T., Gozzi, A., Bernhardt, B.C., Yeo, B.T.T., Milham, M.P., Di Martino, A., 2020. Toward Neurosubtypes in autism. Biol. Psychiatry 88 (1), 111–128.
Kaboodvand, N., van den Heuvel, M.P., Fransson, P., 2019. Adaptive frequency-based modeling of whole-brain oscillations: predicting regional vulnerability and hazardousness rates. Network Neuroscience 3 (4), 1094–1120.
Kaboodvand, N., Iravani, B., Fransson, P., 2020. Dynamic synergetic configurations of resting-state networks in ADHD. NEUROIMAGE 207.
Kennel, M., Brown, R., Abarbanel, H., 1992. Determining embedding dimension for phase-space reconstruction using a geometrical construction. Phys. Rev. A: At. Mol. Opt. Phys. 45 (6), 3403–3411.
Kim, S.H., 2020. Decomposing heterogeneity in autism Spectrum disorder through Neurosubtyping. Biol. Psychiatry 87 (12), E37–E38.
Lai, M.C., Lombardo, M.V., Auyeung, B., Chakrabarti, B., Baron-Cohen, S., 2015. Sex/gender differences and autism: setting the scene for future research. J. Am. Acad. Child Adolesc. Psychiatry 54 (1), 11–24.
Liu, F., Guo, W., Fouche, J.P., Wang, Y., Wang, W., Ding, J., Zeng, L., Qiu, C., Gong, Q., Zhang, W., Chen, H., 2015. Multivariate classification of social anxiety disorder using whole brain functional connectivity. Brain Struct. Funct. 220 (1), 101–115.
Lombardi, A., Guaragnella, C., Amoroso, N., Monaco, A., Fazio, L., Taurisano, P., Pergola, G., Blasi, G., Bertolino, A., Bellotti, R., Tangaro, S., 2019. Modelling cognitive loads in schizophrenia by means of new functional dynamic indexes. NEUROIMAGE 195, 150–164.
Lombardo, M.V., Lai, M.C., Baron-Cohen, S., 2019. Big data approaches to decomposing heterogeneity across the autism spectrum. Mol. Psychiatry 24 (10), 1435–1450.
Lord, C., Risi, S., Lambrecht, L., Cook Jr., E.H., Leventhal, B.L., DiLavore, P.C., Pickles, A., Rutter, M., 2000. The autism diagnostic observation schedule-generic: a standard measure of social and communication deficits associated with the spectrum of autism. J. Autism Dev. Disord. 30 (3), 205–223.
Maenner, M.J., Warren, Z., Williams, A.R., Amoakohene, E., Bakian, A.V., Bilder, D.A., Durkin, M.S., Fitzgerald, R.T., Furnier, S.M., Hughes, M.M., Ladd-Acosta, C.M., McArthur, D., Pas, E.T., Salinas, A., Vehorn, A., Williams, S., Esler, A., Grzybowski, A., Hall-Lande, J., Nguyen, R.H.N., Pierce, K., Zahorodny, W., Hudson, A., Hallas, L., Mancilla, K.C., Patrick, M., Shenouda, J., Sidwell, K., DiRienzo, M., Gutierrez, J., Spivey, M.H., Lopez, M., Pettygrove, S., Schwenk, Y.D., Washington, A., Shaw, K.A., 2023. Prevalence and characteristics of autism Spectrum disorder among children aged 8 years - autism and developmental disabilities monitoring network, 11 sites, United States, 2020. Morbidity and mortality weekly report. Surveillance summaries (Washington, D.C. : 2002) 72(2), 1-14.
Margolis, A.E., Pagliaccio, D., Thomas, L., Banker, S., Marsh, R., 2019. Salience network connectivity and social processing in children with nonverbal learning disability or autism Spectrum disorder. NEUROPSYCHOLOGY 33 (1), 135–143.
Marwan, N., Kurths, J., 2002. Nonlinear analysis of bivariate data with cross recurrence plots. Phys. Lett. A 302 (5), 299–307.
Marwan, N., Romano, M.C., Thiel, M., Kurths, J., 2007. Recurrence plots for the analysis of complex systems. Physics Reports-Review Section of Physics Letters 438 (5–6), 237–329.
Menon, V., Uddin, L.Q., 2010. Saliency, switching, attention and control: a network model of insula function. Brain Struct. Funct. 214 (5–6), 655–667.
Menon, V., Gallardo, G., Pinsk, M.A., Nguyen, V.D., Li, J.R., Cai, W.D., Wassermann, D., 2020. Microstructural organization of human insula is linked to its macrofunctional circuitry and predicts cognitive control. Elife 9.
Napolitano, A., Schiavi, S., La Rosa, P., Rossi-Espagnet, M.C., Petrillo, S., Bottino, F., Tagliente, E., Longo, D., Lupi, E., Casula, L., Valeri, G., Piemonte, F., Trezza, V., Vicari, S., 2022. Sex differences in autism Spectrum disorder: diagnostic, neurobiological, and behavioral features. Front. Psych. 13, 889636.
Nomi, J.S., Farrant, K., Damaraju, E., Rachakonda, S., Calhoun, V.D., Uddin, L.Q., 2016. Dynamic functional network connectivity reveals unique and overlapping profiles of insula subdivisions. Human Brain Mapping 37 (5), 1770–1787.
Nomi, J.S., Uddin, L.Q., 2015. Developmental changes in large-scale network connectivity in autism. NEUROIMAGE-CLINICAL 7, 732–741.
Nomi, J.S., Bolt, T.S., Ezie, C.E.C., Uddin, L.Q., Heller, A.S., 2017. Moment-to-moment BOLD signal variability reflects regional changes in neural flexibility across the lifespan. J. Neurosci. 37 (22), 5539–5548.
Odriozola, P., Uddin, L.Q., Lynch, C.J., Kochalka, J., Chen, T.W., Menon, V., 2016. Insula response and connectivity during social and non-social attention in children with autism. Soc. Cogn. Affect. Neurosci. 11 (3), 433–444.
Pezzimenti, F., Han, G.T., Vasa, R.A., Gotham, K., 2019. Depression in youth with autism Spectrum disorder. Child and Adolescent Psychiatric Clinics Of North America 28 (3), 397−+.
Power, J.D., Barnes, K.A., Snyder, A.Z., Schlaggar, B.L., Petersen, S.E., 2012. Spurious but systematic correlations in functional connectivity MRI networks arise from subject motion. Neuroimage 59 (3), 2142–2154.
Rangaprakash, D., Hu, X., Deshpande, G., 2013. Phase synchronization in brain networks derived from correlation between probabilities of recurrences in functional MRI data. Int. J. Neural Syst. 23 (2), 1350003.
Rim, S.J., Kwak, K., Park, S., 2023. Risk of psychiatric comorbidity with autism spectrum disorder and its association with diagnosis timing using a nationally representative cohort. Res. Autism Spectr. Disord. 104.
Roulston, M.S., 1999. Estimating the errors on measured entropy and mutual information. Physica D: Nonlinear Phenomena 125 (3), 285–294.
Rousseeuw, P.J., 1987. Silhouettes: a graphical aid to the interpretation and validation of cluster analysis. J. Comput. Appl. Math. 20.
Satterthwaite, T.D., Wolf, D.H., Loughead, J., Ruparel, K., Elliott, M.A., Hakonarson, H., Gur, R.C., Gur, R.E., 2012. Impact of in-scanner head motion on multiple measures of functional connectivity: relevance for studies of neurodevelopment in youth. Neuroimage 60 (1), 623–632.
Schaer, M., Kochalka, J., Padmanabhan, A., Supekar, K., Menon, V., 2015. Sex differences in cortical volume and gyrification in autism. Mol. Autism. 6, 42.
Schölkopf, B., Smola, A.J., 2018. Learning with Kernels: Support Vector Machines, Regularization, Optimization, and beyond. The MIT Press.
Seeley, W.W., Menon, V., Schatzberg, A.F., Keller, J., Glover, G.H., Kenna, H., Reiss, A.L., Greicius, M.D., 2007. Dissociable intrinsic connectivity networks for salience processing and executive control. J. Neurosci. 27 (9), 2349–2356.
Shine, J.M., Bissett, P.G., Bell, P.T., Koyejo, O., Balsters, J.H., Gorgolewski, K.J., Moodie, C.A., Poldrack, R.A., 2016. The dynamics of functional brain networks: integrated network states during cognitive task performance. NEURON 92 (2), 544–554.
Syriopoulou-Delli, C.K., Papaefstathiou, E., 2019. Review of cluster analysis of phenotypic data in autism Spectrum disorders: distinct subtypes or a severity gradient model? Int J Dev Disabil 66 (1), 13–21.
Toma, C., 2020. Genetic variation across phenotypic severity of autism. Trends Genet. 36 (4), 228–231.
Uddin, L.Q., 2015. Salience processing and insular cortical function and dysfunction. Nat. Rev. Neurosci. 16 (1), 55–61.
Uddin, L.Q., Supekar, K., Lynch, C.J., Khouzam, A., Phillips, J., Feinstein, C., Ryali, S., Menon, V., 2013. Salience network-based classification and prediction of symptom severity in children with autism. JAMA Psychiatry 70 (8), 869–879.
Uddin, L.Q., Supekar, K., Lynch, C.J., Cheng, K.M., Odriozola, P., Barth, M.E., Phillips, J., Feinstein, C., Abrams, D.A., Menon, V., 2015. Brain state differentiation and behavioral inflexibility in autism. Cereb. Cortex 25 (12), 4740–4747.
Uhlhaas, P.J., Singer, W., 2012. Neuronal dynamics and neuropsychiatric disorders: toward a translational paradigm for dysfunctional large-scale networks. NEURON 75 (6), 963–980.
Urchs, S.G.W., Tam, A., Orban, P., Moreau, C., Benhajali, Y., Nguyen, H.D., Evans, A.C., Bellec, P., 2022. Functional connectivity subtypes associate robustly with ASD diagnosis. ELIFE 11.
Vyas, S., Golub, M.D., Sussillo, D., Shenoy, K.V., 2020. Computation through neural population dynamics. Annu. Rev. Neurosci. 43, 249–275.
Wang, B., Mezlini, A.M., Demir, F., Fiume, M., Tu, Z.W., Brudno, M., Haibe-Kains, B., Goldenberg, A., 2014. Similarity network fusion for aggregating data types on a genomic scale. Nat. Methods 11 (3), 333–U319.
Watanabe, T., Rees, G., 2017. Brain network dynamics in high-functioning individuals with autism. Nat. Commun. 8.
Yan, C., Zang, Y., 2010. DPARSF: a MATLAB toolbox for "pipeline" data analysis of resting-state fMRI. Front. Syst. Neurosci. 4.
Yan, C.-G., Cheung, B., Kelly, C., Colcombe, S., Craddock, R.C., Di Martino, A., Li, Q., Zuo, X.-N., Castellanos, F.X., Milham, M.P., 2013. A comprehensive assessment of regional variation in the impact of head micromovements on functional connectomics. NeuroImage 76, 183–201.
Zhao, L., Xue, S.-W., Sun, Y.-K., Lan, Z., Zhang, Z., Xue, Y., Wang, X., Jin, Y., 2022. Altered dynamic functional connectivity of insular subregions could predict symptom severity of male patients with autism spectrum disorder. J. Affect. Disord. 299, 504–512.